A Numerical Simulation of Three-Dimensional Flow in an Adaptive Wall Wind Tunnel

J. P. Mendoza

A Numerical Simulation of Three-Dimensional Flow in an Adaptive Wall Wind Tunnel

J. P. Mendoza

Ames Research Center
Moffett Field, California

SYMBOLS

a^{ij} — influence coefficient, $\Delta w^i/\Delta w_P^j$ influence coefficient matrix

b^{ij} — element of the inverse matrix

$(a^{ij})^{-1}$ — inverse of matrix a^{ij}

b — wing span, cm

C_L — lift coefficient

$\bar{c}$ — mean aerodynamic chord, cm

M_∞ — free-stream Mach number

MSE — mean square error, $\sqrt{\dfrac{1}{n}\displaystyle\sum_{i=1}^{n}(\Delta w^i)^2}$

w — vertical velocity normalized by the free-stream velocity

w_P — normalized vertical velocity through panel centroid

x,y,z — Cartesian coordinates

α — angle of attack, deg

Δw — difference in vertical velocities

Δw^i — difference in vertical velocities at the ith field level control point

Δw_P^j — difference in vertical velocities at the jth panel centroid

ϕ — perturbation potential function

ϕ_x, ϕ_y, ϕ_z — $\partial\phi/\partial x$, $\partial\phi/\partial y$, $\partial\phi/\partial z$

$\phi_{xx}, \phi_{yy}, \phi_{zz}$ — $\partial^2\phi/\partial x^2$, $\partial^2\phi/\partial y^2$, $\partial^2\phi/\partial z^2$

SUMMARY

Numerical simulations of three-dimensional flows in a prototype adaptive wall wind tunnel were conducted at the Mach number of 0.6 to investigate: (1) wind-tunnel wall interference, (2) active streamline control by varying air removal or injection along the walls, and (3) to develop a method for establishing wall boundary conditions for interference-free flows. It was found that wind-tunnel wall interference could be controlled by using only the vertical velocity components. For the configuration tested, it was found that interference-free flow with solid sidewalls can be approximated by using only floor and ceiling blowing/suction.

INTRODUCTION

The adverse effects of wind-tunnel wall interference have always been considered an important factor in wind-tunnel testing. An early scheme to reduce wall interference in high-speed flow (refs. 1 and 2) involved the use of inserts to conform to a theoretically determined interference-free wall geometry. Later (ref. 3), jacks at several stations along the floor and ceiling were used to shape flexible walls to theoretically determined contours. These early efforts to reduce wall interference were soon discontinued because the calculations that were required to obtain the required wall contours were too laborious. Experimental studies in wind-tunnel wall interference have recently resumed. Present day investigations differ from those of the early forties principally in the use of the adaptive-wall method introduced by Ferri and Baronti (ref. 4) and Sears (ref. 5). The concept, which was made practicable by the use of high-speed computers, is to measure two different flow quantities (such as the axial and vertical components of the velocity along a given line or plane) in the wind tunnel. One of the flow quantities is used to compute the interference-free values of the other quantity by using certain functional relationships that exist between the two quantities. For example, in one application (ref. 5) measured axial velocities were used to compute vertical velocities, the differences between the computed and measured vertical velocities being a measure of the wind-tunnel wall interference. Wall boundary conditions are adjusted and wall interference is re-assessed. This process is repeated until the differences between the measured and computed velocities are sufficiently small so that the flow is essentially interference free.

There are two main methods currently being used to adjust the wall boundary conditions. The streamlined-wall method (refs. 6 to 11) uses a series of jacks for control of the wall contour. The second method attempts to effect streamline changes within the flow by actual blowing or suction at the ventilated walls of the tunnel (refs. 12 to 19). The adaptive-wall studies in the Aerodynamics Division of Ames Research Center have concentrated on the latter approach (refs. 20 and 21).

The method adopted to assess wall interference (ref. 22) uses one measured flow quantity at two surfaces to assess residual wall interference. The method has been successfully demonstrated in two dimensions and an extension to three-dimensional flow has been reported in reference 21.

Because of the many parameters that are involved in the design of three-dimensional adaptive-wall wind tunnels, it is important to simulate the iterative process that would be followed in the wind tunnel as faithfully as is possible. In reference 23, two-dimensional and axisymmetric computer simulations of the adaptive-wall wind tunnel were used to demonstrate a "one-step iteration" to interference-free flow. In this paper, a new computer simulation is described and is used to drive the wind-tunnel flow to an interference-free flow condition without any a priori knowledge of the wall boundary conditions.

A theoretical investigation is conducted here in numerical flow simulations on a semispan wing that is mounted on the sidewall of an adaptive-wall wind tunnel. The flow simulations were conducted at $M_\infty = 0.6$ at two angles of attack, $1°$ and $2°$. The computer code (outer flow solver) that was developed for the present study will be used to develop a numerical adaptive wall simulator for configuration design studies of a new adaptive-wall wind tunnel.

METHOD

Implementation of the adaptive-wall wind-tunnel concept (refs. 4 and 5) requires: (1) measurement of flow variables; (2) assessment of wind-tunnel wall interference; and

(3) adjustment of wall boundary conditions. These steps are repeated until interference-free flow, as computed in step (2) above, is indicated. The operation of an adaptive-wall wind tunnel can be represented by the flow diagram shown in figure 1. Measurements of the flow variables are made in the wind tunnel at two imaginary planar surfaces surrounding the model. The measurements on the planar surface that is closest to the model (the source level) are used as inputs to the wall-interference assessment program from which the values for Δw are computed, the values being the differences between the vertical velocities that are computed by the outer flow solver and those at the planar surface farthest from the model (the field level). If the values for Δw satisfy the convergence criteria, the operation is terminated; otherwise, they are used as inputs to the influence coefficient program to determine a new set of wall boundary conditions (Δw^P) for the wind tunnel. The blocks labeled "wind-tunnel flow field," "wall-interference assessment," and "influence coefficient" will be discussed in more detail.

Wind-Tunnel Flow Field

The wind-tunnel flow field is modeled by a particular solution to Laplace's equation

$$\phi_{xx} + \phi_{yy} + \phi_{zz} = 0 \qquad (1)$$

Although a number of computer programs are available to solve the potential flow equation with wind-tunnel boundary conditions, the Douglas-Neumann Potential Flow Computer Program (ref. 24) was selected for this study because it has the following features: (1) the program can be applied to complex configurations; (2) the user can specify velocities on the surface of the configuration being studied; and (3) the user can specify points in the flow field where the flow quantities are to be computed. The computer program is a "panel code" that uses the Gothert transformation to account for the effects of compressibility (Mach number).

The wind tunnel paneling scheme is shown in figure 2. The wind tunnel is 53-cm long, 25-cm wide, and 13-cm high. These dimensions model the Ames adaptive-wall wind tunnel used in the experiments reported in references 20 and 21. The surfaces of the wind tunnel were represented by 168 panels. The floor and ceiling surfaces were each represented by 36 panels (three panels in the lateral direction and twelve panels in the longitudinal direction) and each of the sidewalls were represented by 48 panels (four panels in the vertical direction and twelve panels in the longitudinal direction). The wing (fig. 3) was supported from one sidewall (which serves as a reflecting plane) with its leading edge at two chord lengths from the upstream-end of the test section. It was represented by 200 panels on each of the upper and lower surfaces. The coordinate system used in this investigation is shown in figure 4.

Although three velocity components may be specified at any of the panel centroids, only velocities normal to the floor and ceiling panels were introduced as boundary conditions in the current study. (These velocities were meant to simulate actual blowing or suction at the floor and ceiling of the wind tunnel.) It was assumed that solid sidewalls were used in this investigation. Figure 5 shows a typical vertical velocity distribution (at $2y/b = 0.71$, $z/\bar{c} = 0.63$) induced by blowing through a singles point in the ceiling (tunnel empty) at $M_\infty = 0.6$ where the blowing was simulated by a source at the panel centroid.

Wall Interference Assessment

The method of assessing wind-tunnel wall interference in this study follows the one described in reference 22 which used only the vertical velocity component. In solving the "wing-in-the-wind-tunnel" problem, vertical velocities were computed at control points on two different imaginary planar surfaces (the source and field levels) that enclosed the model (fig. 6). The field level control points are at $x/\bar{c} = -0.69, -0.46, -0.23, 0., 0.23, 0.46, 0.69, 0.92$, and 1.15. The point $x/\bar{c} = 0$ is at $\bar{c}/4$. The lateral spacing of the control points is $2y/b = 0.24, 0.71, 1.18$, and 1.30. The vertical spacing is $z/\bar{c} = \pm0.52$ and 0.0. Using the vertical velocities on the surface closest to the model (source level) the vertical velocities on the other surface (the field level) were calculated by solving a second potential flow problem (the "outer-flow solution"). Specifically, the vertical velocities, $\phi_z = w$, on the source level together with the far-field boundary conditions, $\phi_x = \phi_y = \phi_z = 0$, are used to numerically solve the compressible small-disturbance equation

$$(1 - M_\infty^2)\phi_{xx} + \phi_{yy} + \phi_{zz} = 0 \qquad (2)$$

The solution to this second potential flow problem (the outer flow solution) is used to compute the vertical velocities on the field level surface. The differences between the previously computed vertical velocities on the field level surfaces and those computed using the outer flow solver are a measure of wall interference. When these differences are sufficiently small, the flow can be considered interference free. In this study the mean square error (MSE) based on the differences between the vertical velocities that are computed by the method in reference 24 and those that are computed by the outer flow solver was used as a measure of the residual interference. When this parameter is less than or equal to a given minimum value, then the flow is considered to be interference free. The minimum values (see appendix) are 0.493×10^{-3} for the upper and lower field level surfaces ($z/\bar{c} = 0.52$) and 1.099×10^{-3} for the station that is outboard of the wing tip ($z/\bar{c} = 0$). (In this study all the velocities have been normalized by the free-stream velocity.) The minimum values for the MSEs are discussed further in the appendix;

Influence Coefficients

The method of influence coefficients used in the present study follows the method first used experimentally in reference 20. Basically, an efficient method is needed to determine the required increment in the boundary conditions at each of the floor and ceiling panels when the increment in vertical velocities is given at each of the control points on the field level surface. Specifically, the change in the velocity, Δw^i, at the ith field level control point is equal to a linear combination of the velocities, Δw^i_p, through the floor and ceiling panels. This is expressed by the equation

$$
\begin{bmatrix} \Delta w^1 \\ \Delta w^2 \\ \vdots \\ \Delta w^m \end{bmatrix} = \begin{bmatrix} a^{11} & a^{12} & \ldots & a^{1m} \\ a^{21} & a^{22} & \ldots & a^{2m} \\ \vdots & \vdots & & \vdots \\ a^{m1} & a^{m2} & \ldots & a^{mm} \end{bmatrix} \begin{bmatrix} \Delta w^1_P \\ \Delta w^2_P \\ \vdots \\ \Delta w^m_P \end{bmatrix} \quad (3)
$$

Here, the a^{ij} are the influence coefficients which are assumed invariant with each iteration. The procedure for determining the a^{ij} is as follows: velocities (Δw^i_p) were specified at one pair (in this case the jth pair) of opposite-facing floor and ceiling panels. Flow entered the test section (blowing) at the floor and exited (suction) through the ceiling at a single pair (the jth pair) of floor and ceiling panels. The velocities, Δw^1, Δw^2, ..., Δw^m that were induced at the field level control points were used to compute influence coefficients, $a^{ij} = \Delta w^i / \Delta w^j_p$, column by column. Assuming that there is an equal number of control points and panels, the a^{ij}-matrix in equation (3) is square and may be readily inverted. Assuming that an inverse matrix $(a^{ij})^{-1}$ exists, then the following equation can be obtained by multiplying both sides of equation (3) by $(a^{ij})^{-1}$.

$$
\begin{bmatrix} \Delta w^1_P \\ \Delta w^2_P \\ \vdots \\ \Delta w^m_P \end{bmatrix} = \begin{bmatrix} b^{11} & b^{12} & \ldots & b^{1m} \\ b^{21} & b^{22} & \ldots & b^{2m} \\ \vdots & \vdots & & \vdots \\ b^{m1} & b^{m2} & \ldots & b^{mm} \end{bmatrix} \begin{bmatrix} \Delta w^1 \\ \Delta w^2 \\ \vdots \\ \Delta w^m \end{bmatrix} \quad (4)
$$

The left-hand side of this equation represents the vectors of the required wall panel velocities and $b^{ij} = (a^{ij})^{-1}$. When the values for a^{ij} were computed, it was found that the strongest influences were produced by the blowing or suction on the nearest wall panel. For example, the field level control points that were closest to the ceiling were quite insensitive to the flows through the floor panels. This effectively decoupled the control of the upper and lower halves of the test section.

A similar result was reported in the experimental investigation in reference 20. It was also found that the subset of panels shown in figure 7 produced the strongest influence on the velocities at the field level control points depicted by the crosses. The induced velocities from the other panels were so small that they were neglected. The final influence coefficient matrix was an 18 by 18 array.

RESULTS AND DISCUSSION

The first part of the present investigation was to establish procedures for effecting interference-free flows in the wind tunnel. This was done with the wing at $2°$ angle of attack. The second part was to apply those procedures to the same wing at $1°$ angle of attack. The Douglas-Neumann code failed when applied to the $\alpha = 3°$ case.

A natural starting point for the beginning of the adaptive-wall wind-tunnel operation would be the computation of the solid-wall wind-tunnel flow characteristics. Figure 8 shows the vertical velocity distributions that are computed at the field level control points and those that are computed by using the outer flow solver. Note the large wall interference effects that are indicated by the Δw-differences between the two sets of data. The cross sectional location of each pair of curves is shown by the cross in the inset. Using the outer flow solution as the standard for comparison, it is observed that for the Δw-differences to vanish, the magnitudes of the solid-wall vertical velocities must increase at all field level control points except for those that are outboard of the wing tip $(z/\bar{c} = 0)$. Here reductions in the magnitudes of w are indicated. The problem is to determine a set of boundary conditions on the floor and ceiling panels outboard of the wing tip which will increase the magnitudes of the vertical velocities at $2y/b = 1.18$ $(z/\bar{c} = 0.52)$ and which will decrease the magnitudes of the velocities at $2y/b = 1.30$ $(z/\bar{c} = 0)$. This problem, which may not exist in an actual wind-tunnel experiment, may be associated with the method (Douglas-Neumann Program) for computing the flow-field characteristics near the wing tip. Since the appropriate course of action is not known beforehand, the vertical velocities at $z/\bar{c} = 0$ were neglected (for the time being) and the primary consideration was given to eliminating wall interference effects at the other control points. As previously mentioned, an iterative procedure would be followed, and at each iteration the Δw-differences would be used as inputs to the influence coefficient program to determine the wall boundary conditions.

Figure 9 shows the vertical velocity distributions after the first iteration. The wall interference was reduced slightly with a resulting reduction in C_L from 0.218 to 0.204.

After four iterations a set of vertical velocity distributions were obtained showing little or no wall interference at nearly all of the field control points. Figure 10 shows the vertical

3

velocity distributions after the four iterations. The data at the $z/\bar{c} = \pm0.52$-control points show little or no indications of wall interference. The velocity distributions at the station outboard of the tip ($z/\bar{c} = 0$), however, show that wall interference still persists there. The lift coefficient of 0.181 is higher than the interference-free value of 0.161.

The convergence rate for this sequence of calculations is shown in figure 11. The MSE (mean square error) at each iteration is observed to approach, and finally assume, a value less than that for the interference-free condition. This is in contrast to the MSE of the data outboard of the tip (in the wing plane $z/\bar{c} = 0$) which becomes larger with each iteration (fig. 11(b)). The reason for this is not presently known and will be studied further in later investigations.

Figure 12 shows how C_L was reduced with each iteration. Here it is evident that although most of the data (at all points except at $z/\bar{c} = 0$) showed convergence, the C_L did not match that for free air.

Next, an alternate strategy was employed whereby a new starting point was found (the second set of iterations). This was the result of using boundary conditions which were eight times the blowing and suction velocities for the case shown in figure 9 ($C_L = 0.204$). The magnitudes of the resulting vertical velocities (fig. 13) are observed to be generally greater than those computed using the outer flow solver. The most noteworthy result is that for the Δw values to be able to vanish, the magnitudes of all the adaptive wall w's must be reduced. (A scale change was required for this figure because of the larger magnitudes of the vertical velocities.)

Seven iterations were required to reach interference-free flow conditions. The results of the seventh iteration are shown in figure 14. Note that the lift coefficient is close to that of the free-air value of 0.161.

The convergence rate (fig. 15) shows clearly how the MSE for the data at $z/\bar{c} = \pm0.52$ and those for $z/\bar{c} = 0$ progressed from a large starting value to a smaller and smaller value with each iteration. Although the MSE for the data at the outboard station ($z/\bar{c} = 0$) did not assume a value less than that for free air, it apparently is close enough judging by the close agreement of the C_L to that of the free-air value of 0.161.

Figure 16 shows the effect of iteration on C_L. The data denoted by the circle symbols are from the previously described first set of iterations. The data denoted by the square symbols are the results of the second sequence. Both the MSE and C_L values show that the adaptive wall wind tunnel has effectively achieved free-air conditions.

Figure 17 shows a comparison between the adaptive wall vertical velocities and those for free air. The good agreement shown between the two sets of data verifies the adaptive wall results.

To summarize the previously developed procedure, the iteration must start from a point where the boundary conditions for reducing the Δw-differences is consistent from one set of field level control points to another. For instance, at the control points outboard of the wing tip in figure 8, the boundary conditions were to increase the w's at $z/\bar{c} = \pm0.52$ and, simultaneously to decrease the w's at $z/\bar{c} = 0$. This conflicting requirement is not observed in the data in figure 13 where all the w's have to be reduced for the Δw values to vanish.

The procedures for establishing interference-free flows which were developed for the 2° angle of attack case were applied to the wing at $\alpha = 1°$. Shown in figure 18 are the solid wall vertical velocity distributions and those computed using the outer flow solver. Using the outer flow solver velocities as the standard for comparison, the magnitudes of the solid wall velocities must increase at all of the field level control points except those at the outboard station ($z/\bar{c} = 0$). To find the new starting point, the values for Δw were used as inputs to the influence coefficient program to solve the boundary conditions. These were multiplied by four and imposed as boundary conditions in the Douglas-Neumann program. The resulting vertical velocity distributions including those from the outer flow solution are shown in figure 19. This constituted the starting point from which to begin the iteration. Four iterations were required to achieve interference-free flow conditions. The results of the final iteration are shown in figure 20, where little or no wall interference is indicated (except at $2y/b = 1.30$).

The rate of convergence is shown in figure 21. The final value of the MSE for the data at $z/\bar{c} = \pm0.52$ is below that for free air. The MSE for the data at the points outboard of the wing tip ($z/\bar{c} = 0$) is shown to approach but not to assume values less than that for free air. The lift coefficient for the last iteration is 0.086, while that for free air is 0.081.

Figure 22 shows the effects of iteration for the $\alpha = 1°$ case. The $\alpha = 2°$ iterations are also shown in the figure. Note that although the C_L value was quickly reached, the MSE data indicated that three iterations were required to satisfy the convergence criteria.

Adaptive wall vertical velocity distributions and those for free air are compared in figure 23. The differences between the two sets of data may account for the slight difference in C_L.

CONCLUSIONS

The following conclusions may be drawn from this study:

1. The method of influence coefficients may be used to obtain a succession of boundary conditions that can be used in an iterative scheme to compute interference-free flow in the wind tunnel.

2. The vertical velocities at the upper and lower field level control points may be varied independently of each other by changing the ceiling and floor boundary conditions, respectively. This effectively decouples the upper half from the lower half of the wind tunnel.

3. It is not necessary to introduce blowing/suction at all of the floor and ceiling panels.

4. The simulation described in this report can be used for trade-off studies in the design of three-dimensional adaptive wall wind tunnels.

APPENDIX

For interference-free flow the vertical velocities computed by the outer flow solver would be expected to be identical to those computed by the method of reference 24. However, since the method of finite differences is used to solve the small disturbance equation in the outer flow solver, the accuracy of the solution will depend mainly on the mesh size. In the present investigation the mesh was refined several times until the Δw-differences (shown in fig. 24) between the free air and the outer flow solver data were sufficiently small. Because the Δw-differences at the field level control points at $z/\bar{c} = \pm 0.52$ were much smaller than those at the $z/c = 0$-control points, two convergence criteria were established based on the mean square error. The MSE was specified as 0.493×10^{-3} for the data at $z/\bar{c} = \pm 0.52$ and 1.099×10^{-3} for the data at $z/\bar{c} = 0$. The MSE for the data at $z/\bar{c} = 0$ could have been reduced further by more reduction in mesh size. Since one of the objectives of the present investigation was to find a quick method for assessing wall interference, the results were considered satisfactory so that further mesh size refinement was not required. The criteria adopted herein is the following: the flow is considered interference free if the MSE of the data at $z/\bar{c} = \pm 0.52$ is less than 0.493×10^{-3} and if the MSE of the data at $z/\bar{c} = 0$ is approximately equal to 1.099×10^{-3}.

REFERENCES

1. Preston, J. H.; and Sweeting, N. E.: The Experimental Determination of the Interference on a Large Chord Symmetrical Joukowski Aerofoil Spanning a Closed Tunnel. Aeronautical Research Committee R&M 1997, 1942.

2. Preston, J. H.; Sweeting, W. E.; and Cox, D. K.: The Experimental Determination of the Two-Dimensional Interference on a Large Chord Piercy 12/40 Aerofoil in a Closed Tunnel Fitted with a Flexible Roof and Floor. Aeronautical Research Committee R&M 2007, 1944.

3. Lock, C. N. H.; and Beavan, J. A.: Tunnel Interference at Compressible Speeds Using the Flexible Walls of the Rectangular High Speed Tunnel. Aeronautical Research Committee R&M 2005, 1944.

4. Ferri, A.; and Baronti, P.: A Method for Transonic Wind-Tunnel Corrections. AIAA J., vol. II, no. 1, Jan. 1973.

5. Sears, W. R.: Self Correcting Wind Tunnels, Aeronautical J., vol. 78, Feb./Mar. 1974, pp. 80–89.

6. Wolf, S. W. D.; Cook, I. D.; and Goodyer, M. J.: The Status of Two- and Three-Dimensional Testing in the University of Southampton Transonic Self-Streamlining Wind Tunnel. AGARD Fluid Dynamics Panel Specialists' Meeting on Wall Interference in Wind Tunnels, London, U.K., May 19–20, 1982. AGARD CP-335.

7. Goodyer, M. J.; and Wolf, S. W. D.: The Development of a Self Streamlining Flexible Walled Transonic Test Section. AIAA Paper 80-0440, Mar. 1980, pp. 325–335.

8. Ganzer, U.: Adaptable Wind Tunnel Walls for 2-D and 3-D Model Tests. ICAS Paper 23.3 (revised version), Oct. 1980.

9. Gruzdev, A. A.: On Low-Speed Wind Tunnels with Deformable Boundaries. Izvestiya, VUZ. Aviatsionnaya Tekhnika (translation: Soviet Aeronautics), vol. 23, no. 4, 1980, pp. 18–20.

10. Chavallier, Jean-Pierre: Soufflerie Transonique a Parois Auto-Adaptables. Paper 12, AGARD Conference Proceedings no. 174 on Wind Tunnel Design and Testing Techniques, Oct. 1975.

11. Goodyer, M. J.: A Low Speed Self Streamlining Wind Tunnel. Paper 13, AGARD Conference Proceedings no. 174 on Wind Tunnel Design and Testing Techniques, Oct. 1975.

12. Ganzer, U.: Wind Tunnels with Adapted Walls for Reducing Wall Interference. NASA TM-75501, Aug. 1979.

13. Erickson, J. C., Jr.; Wittlift, C. E.; Padova, C.; and Homicz, G. F.: Adaptive-Wall Wind-Tunnel Investigations. Calspan Report no. RK-6040-A-2, Feb. 1981. AD-A096325.

14. Erickson, J. C., Jr.; and Homicz, G. F.: Numerical Simulations of a Segmented-Plenum, Perforated, Adaptive-Wall Wind Tunnel. AIAA Paper 81-0160, Jan. 1981.

15. Parker, R. L., Jr.; and Sickles, W. L.: Two-Dimensional Adaptive-Wall Experiments. Arnold Engineering Development Center TR-80-63, Feb. 1981. AD-A095199.

16. Parker, R. L., Jr.; and Sickles, W. L.: Application of Adaptive Wall Techniques in a Three Dimensional Wind Tunnel with Variable Wall Porosity. AIAA Paper 80-0157, Jan. 1980.

17. Vidal, R. J.; and Erickson, J. C., Jr.: Experiments on Supercritical Flows in a Self-Correcting Wind Tunnel. AIAA Paper 78-788, April 1978, pp. 130–141.

18. Vidal, R. J.; Erickson, J. C.; and Catlin, P. A.: Experiments with a Self Correcting Wind Tunnel. AGARD Paper 11, Proceedings no. 174 on Wind Tunnel Design and Testing Techniques, Oct. 1975.

19. Kraft, E. M.; and Parker, R. L., Jr.: Experiments for the Reduction of Wind Tunnel Wall Interference by Adaptive Wall Technology. Arnold Engineering Development Center TR-79-51, Oct. 1979. AD-A076555.

20. Satyanarayana, B.; Schairer, E.; and Davis, S.: Adaptive-Wall Wind-Tunnel Development for Transonic Testing. J. of Aircraft, vol. 18, no. 4, April 1981, pp. 273–279.

21. Schairer, Edward T.; and Mendoza, Joel P.: Adaptive-Wall Wind-Tunnel Research at Ames Research Center. Paper No. 16, AGARD Fluid Dynamics Panel Specialists' Meeting on Wall Interference in Wind Tunnels, London, U.K., May 19–20, 1982. AGARD CP-335.

22. Davis, S. S.: A Compatibility Assessment Method for Adaptive Wall Wind Tunnels. AIAA Paper 81-4226, AIAA J., vol. 19, no. 9, Sept. 1981.

23. Lo, C. F.; and Sickles, W. L.: Analytic and Numerical Investigations of the Convergence for the Adaptive Wall Concept. Arnold Engineering Development Center TR-79-55, Nov. 1979.

24. Hess, J. J.: Calculation of Potential Flows About Arbitrary Three Dimensional Lifting Bodies. Douglas Aircraft Company, Inc., Report MDC-J5679-01, Oct. 1972. AD-755480.

7
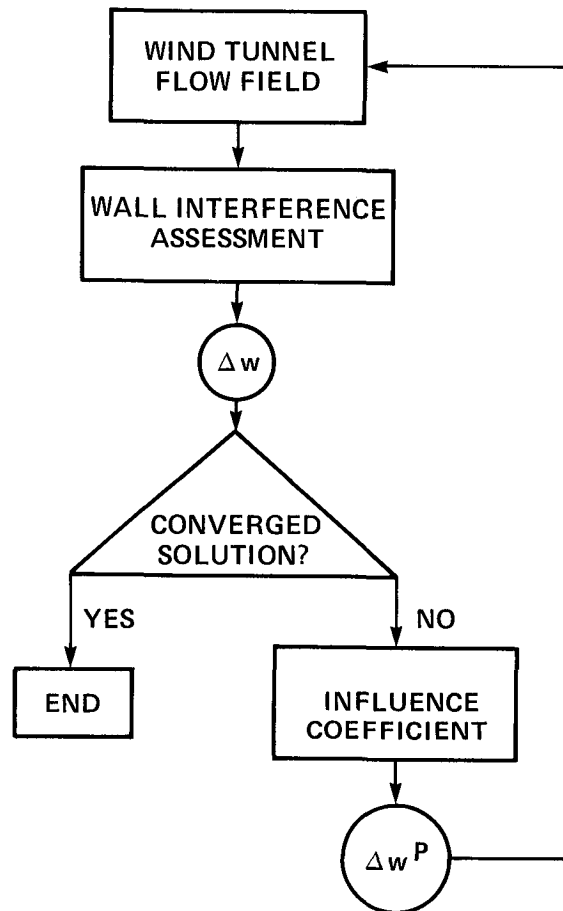
Figure 1.— Adaptive wall wind tunnel operation.
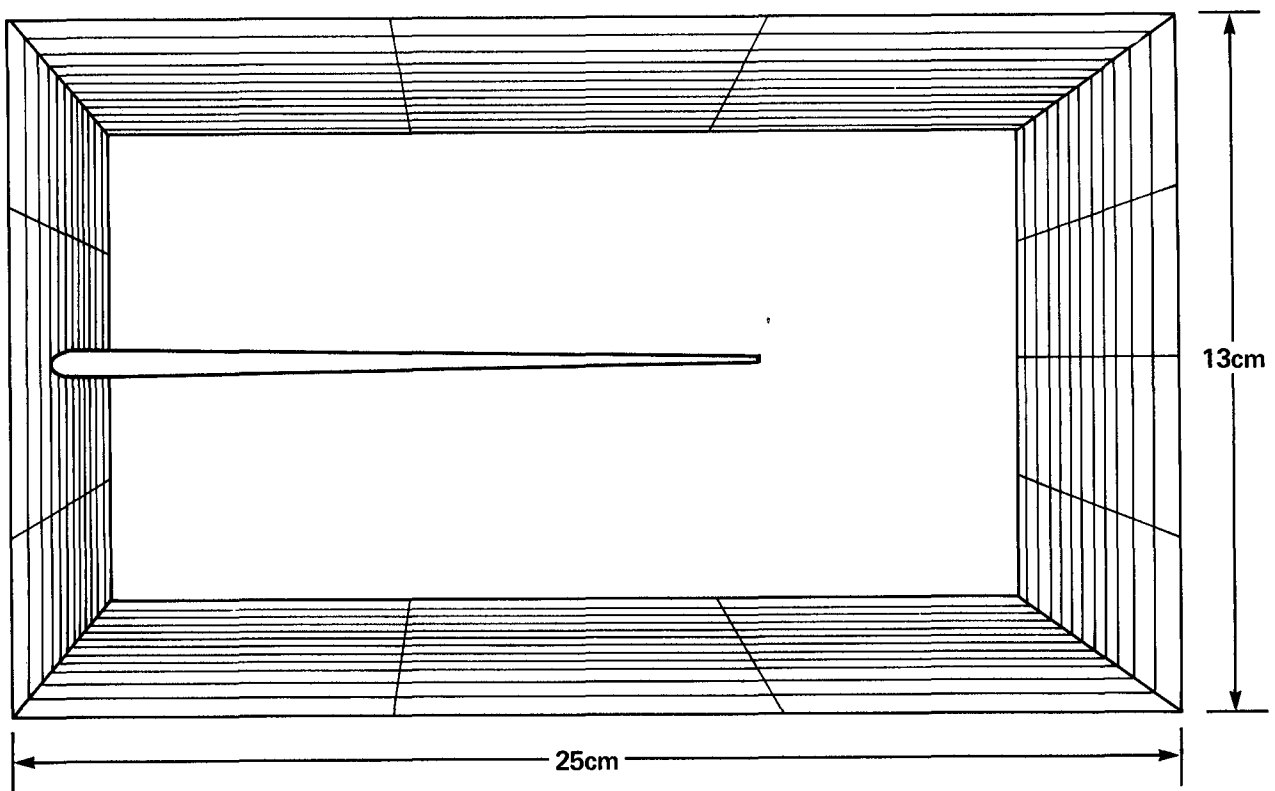
Figure 2.— Wind-tunnel paneling scheme.
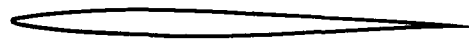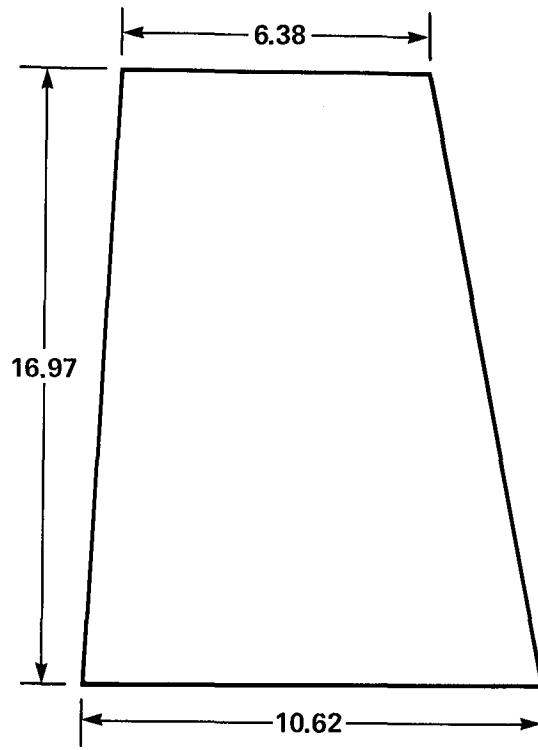
NACA 65A006 SECTION

$\Lambda_{L.E.} = 3.58°$

$\bar{c} = 8.66$ DIMENSIONS IN cm

Figure 3.— Wing geometry.

FLOW DIRECTION

REFERENCE POINT: $\bar{c}/4$
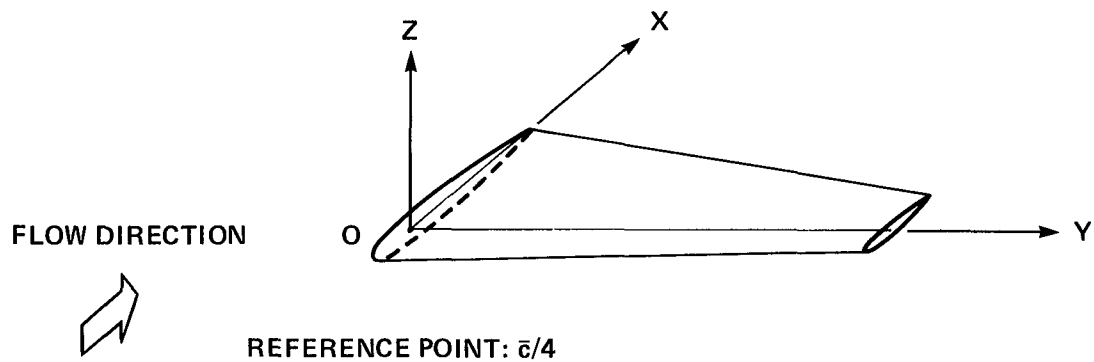
Figure 4.— Coordinate system.

CEILING PANEL

2y/b = 0.71
z/c̄ = 0.63

w

$x/\bar{c}$
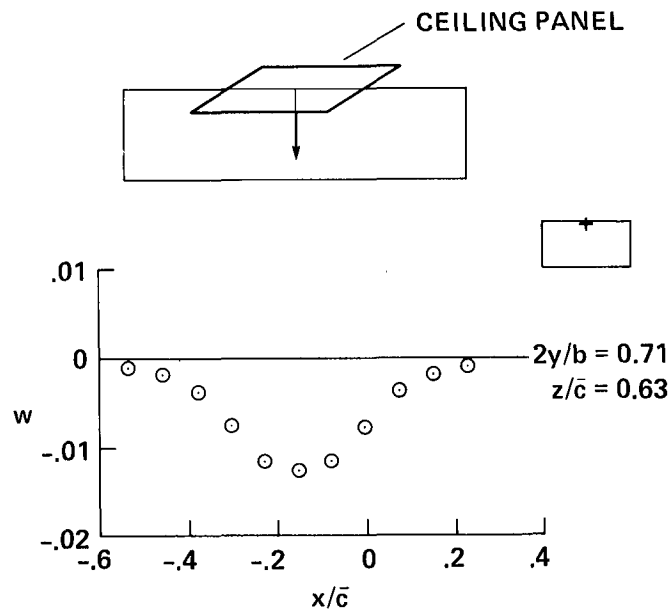
Figure 5.— Vertical velocity distribution induced by blowing through a single panel point, tunnel empty, M = 0.6.

WIND TUNNEL

FIELD LEVEL SURFACE

SOURCE LEVEL SURFACE

WING
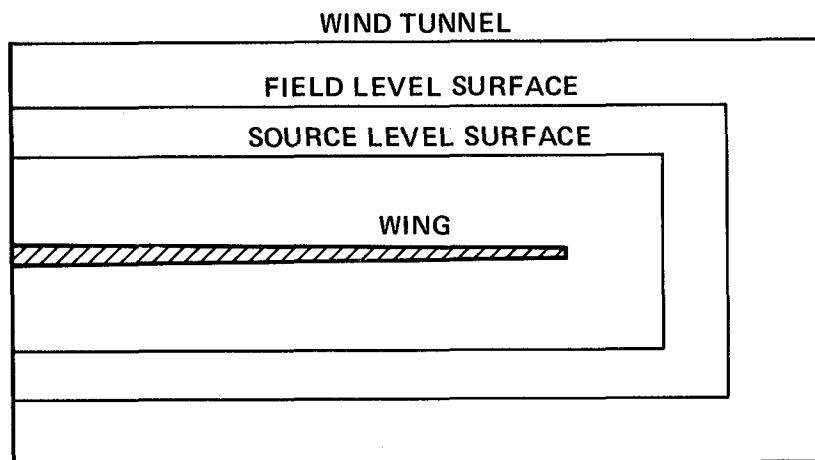
Figure 6.— Cross sectional view of wind tunnel.
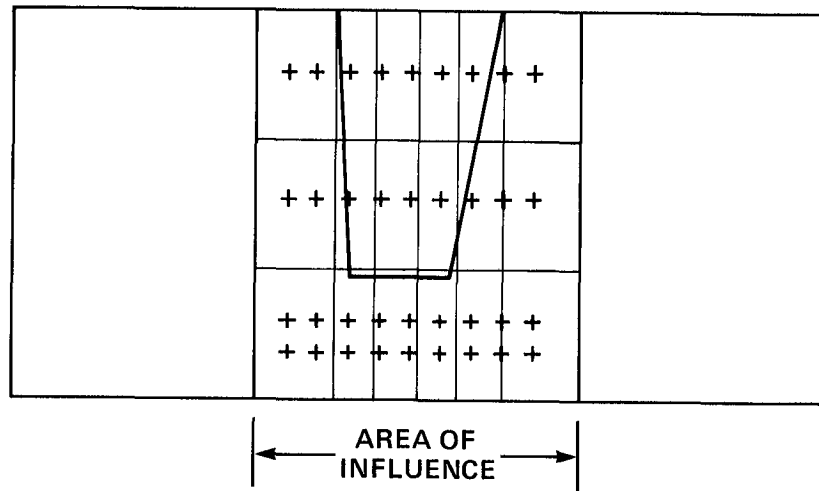
+ FIELD LEVEL CONTROL POINTS

Figure 7.— Wind tunnel layout.
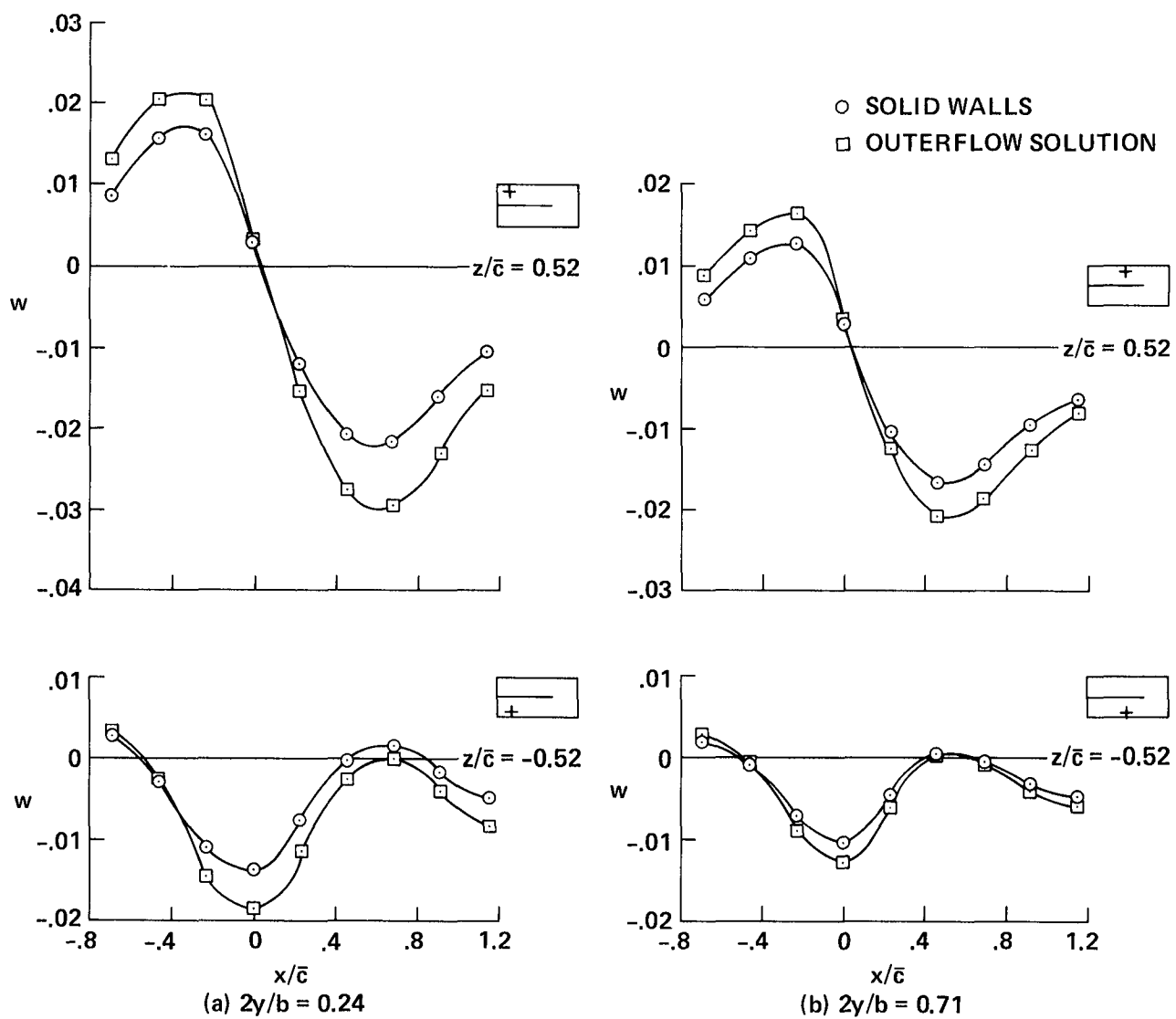
Figure 8.– Vertical velocities for the solid wall wind tunnel, $C_L = 0.218$.
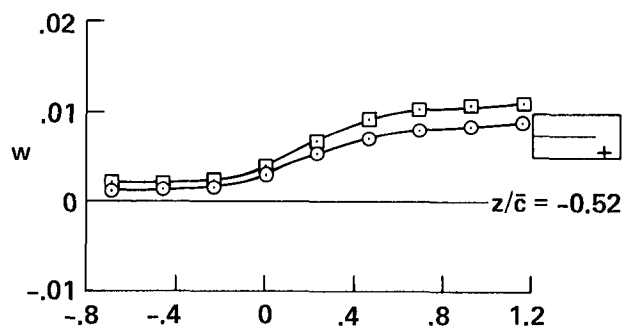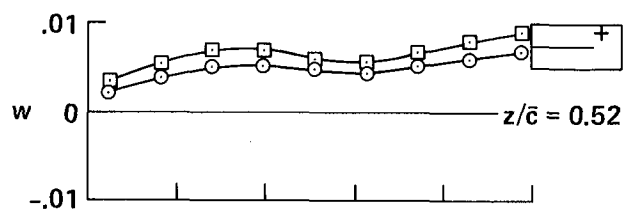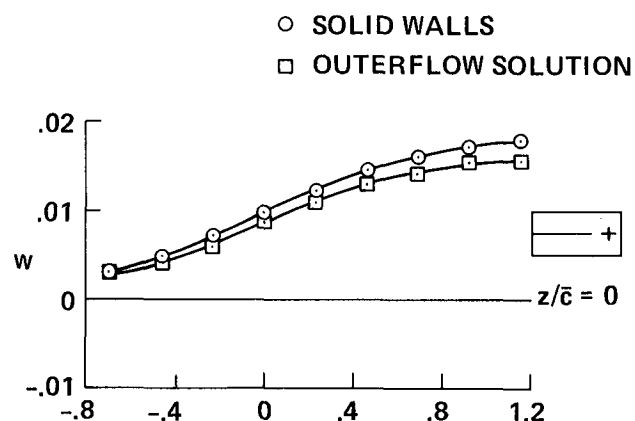
Figure 8.— Concluded.
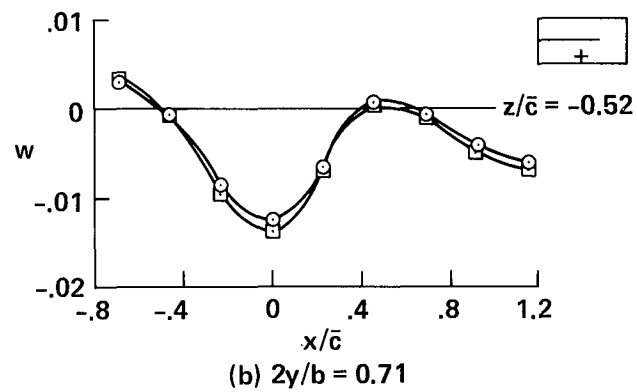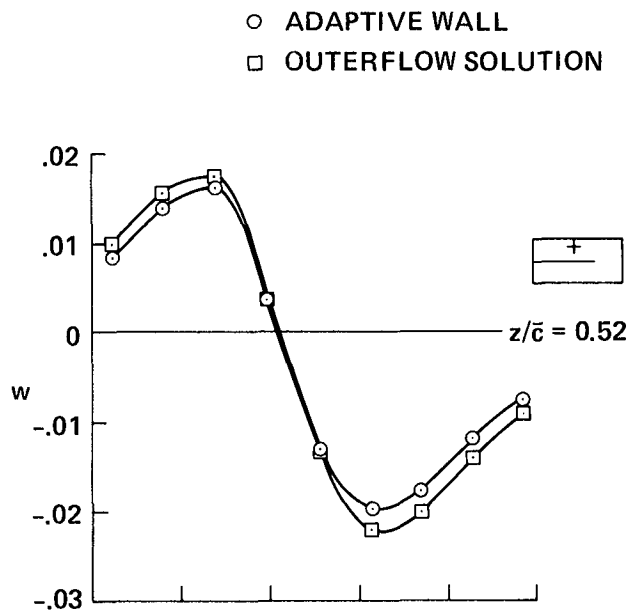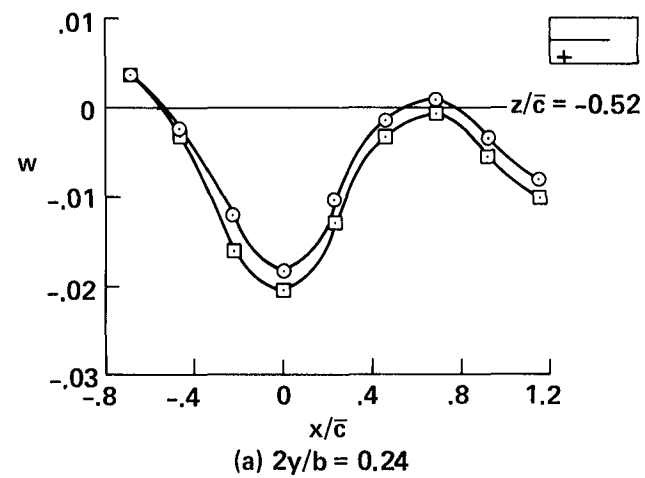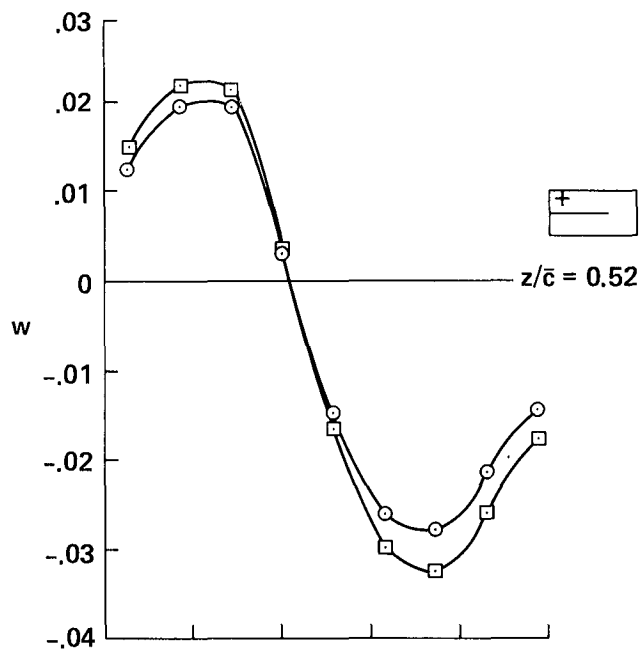
Figure 9.— Vertical velocities for the adaptive wall wind tunnel, first iteration, C_L = 0.204.
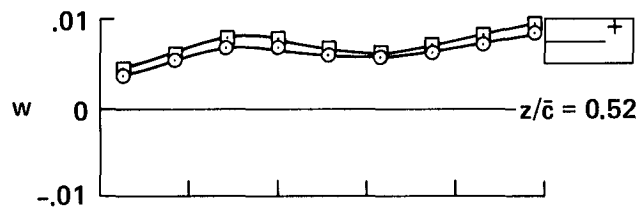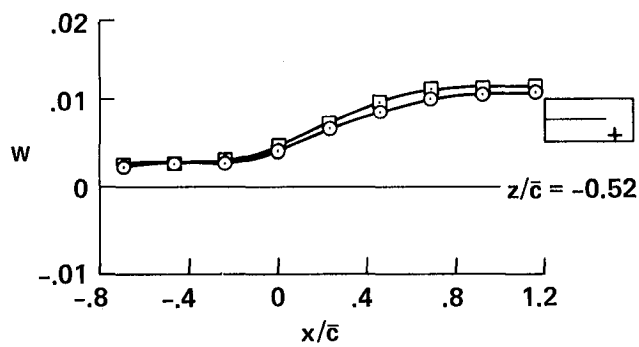
(c) 2y/b = 1.18
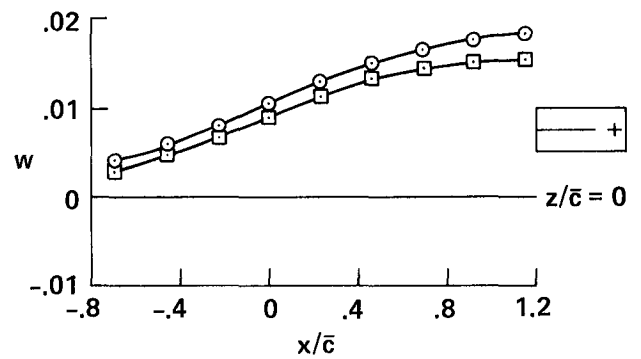
(d) 2y/b = 1.30

Figure 9.— Concluded.
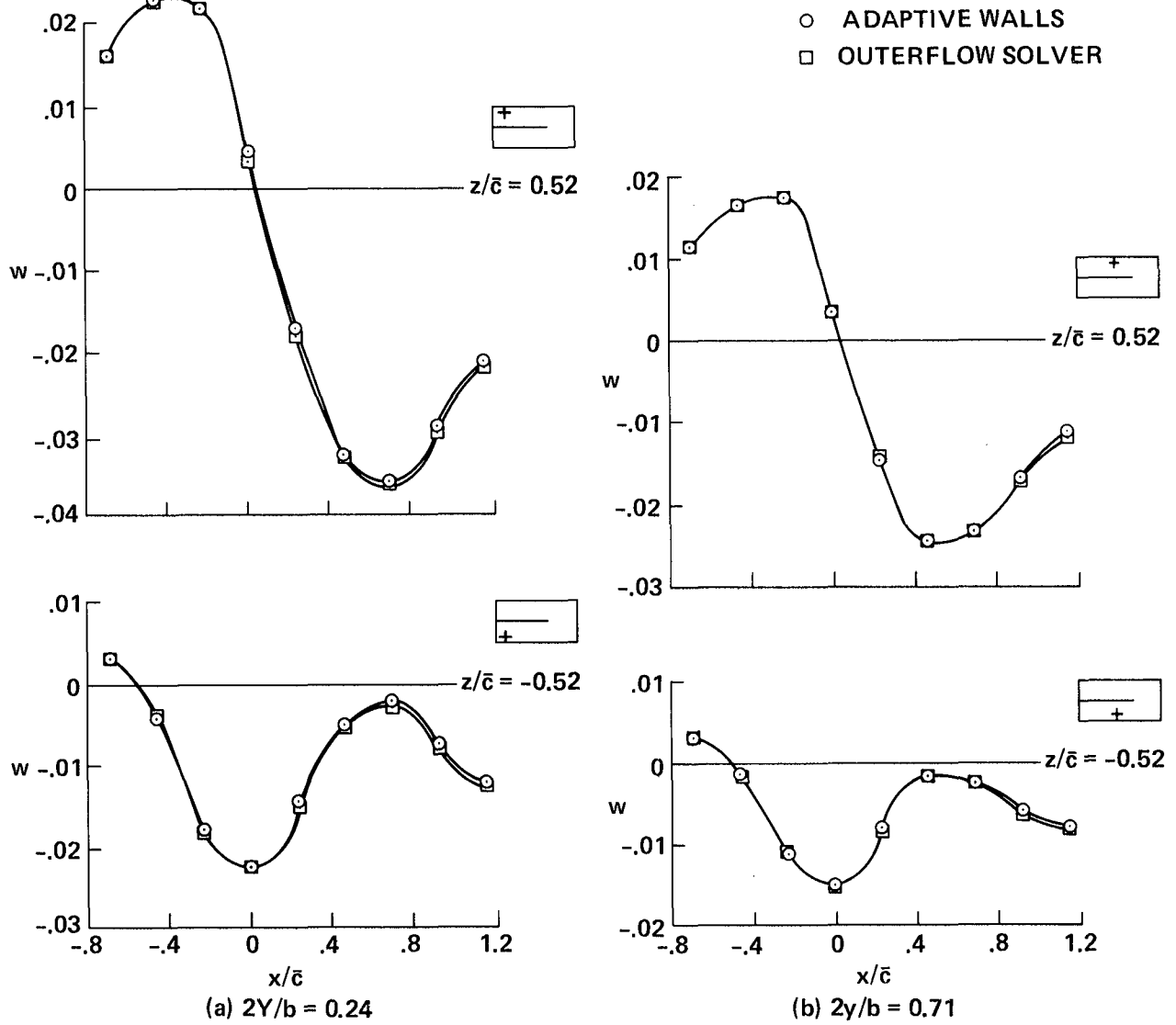
Figure 10.— Vertical velocities for the adaptive-wall wind tunnel, fourth iteration, $C_L = 0.181$.

(c) 2y/b = 1.18

(d) 2y/b = 1.30
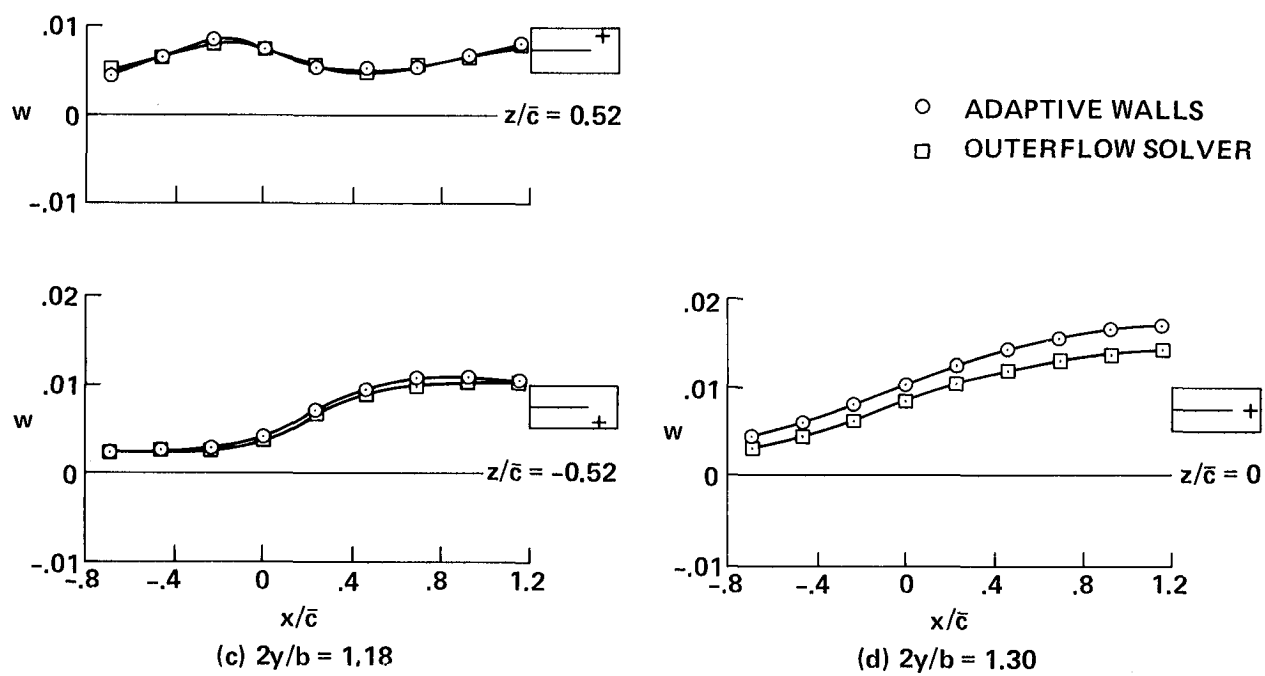
Figure 10.— Concluded.
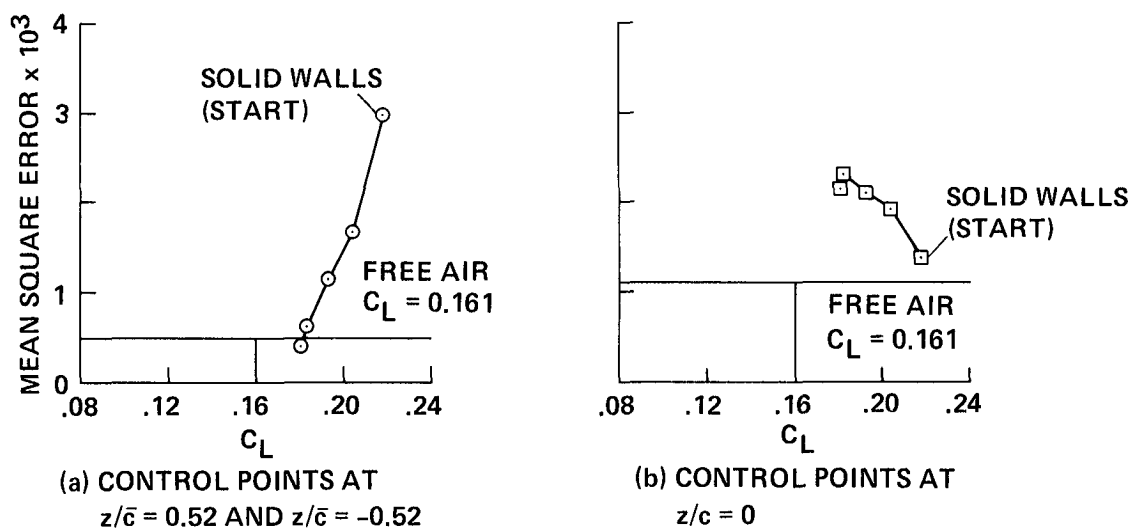
Figure 11.— Convergence rate.
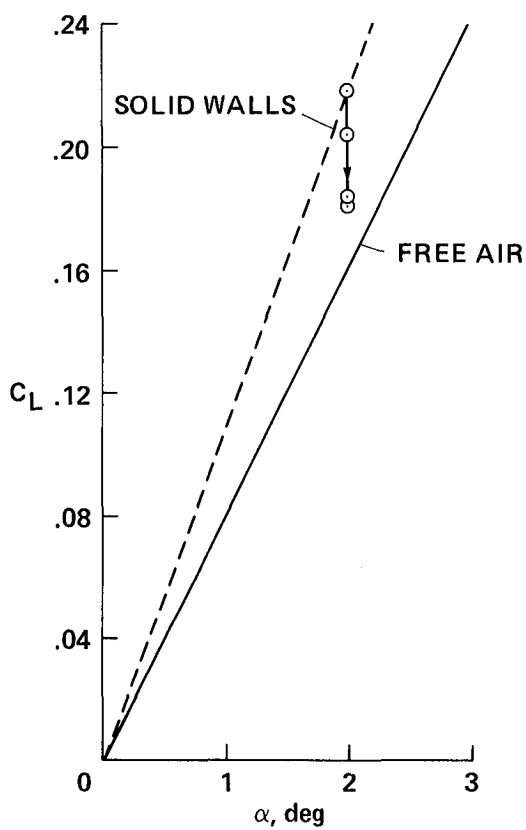
Figure 12.— Effect of iteration on C_L, $\alpha = 2°$.
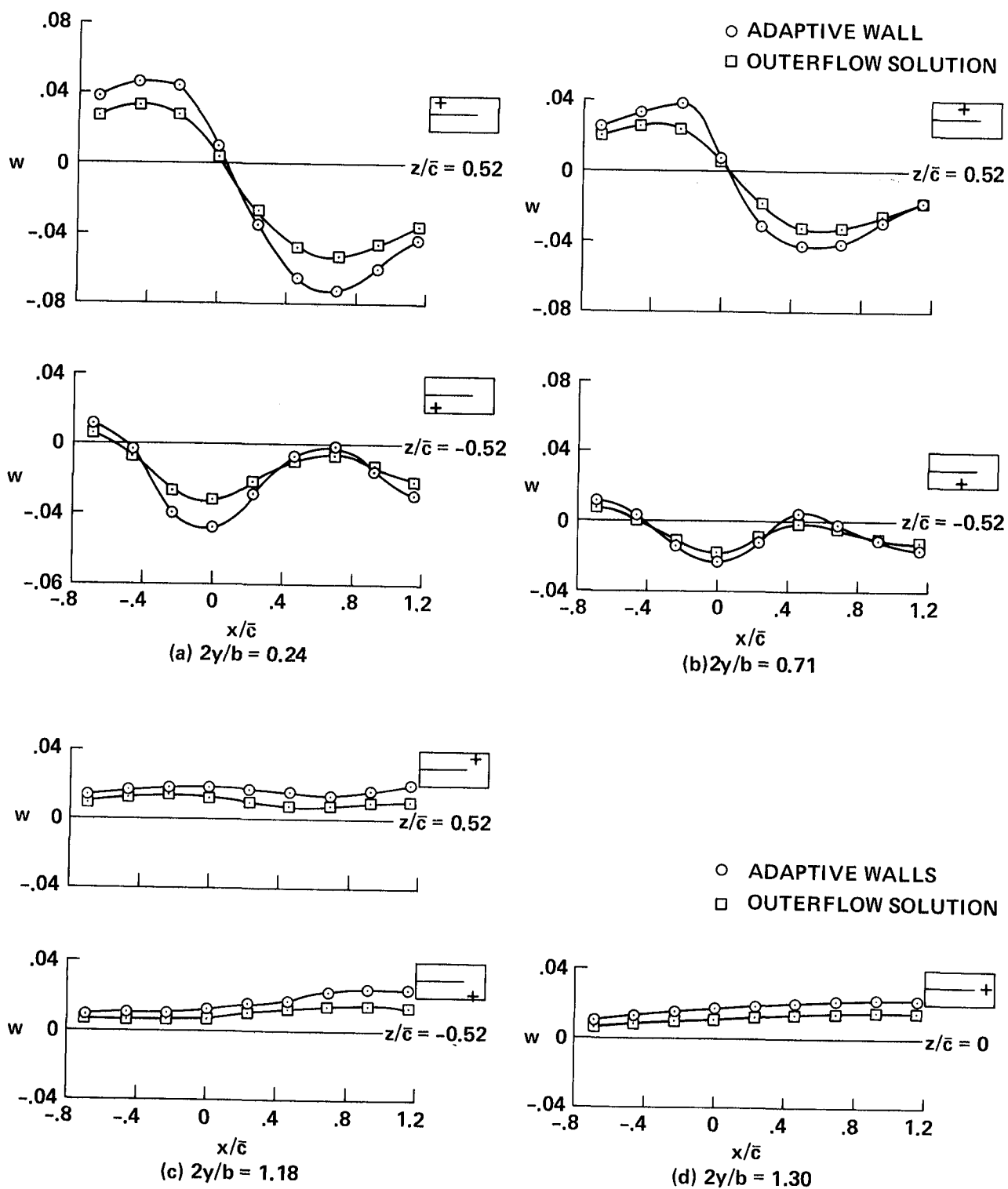
Figure 13.— Vertical velocities for the adaptive-wall wind tunnel second iteration (series 2), $C_L = 0.112$.
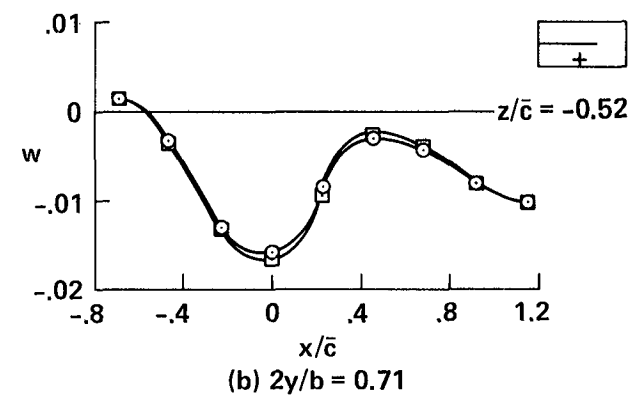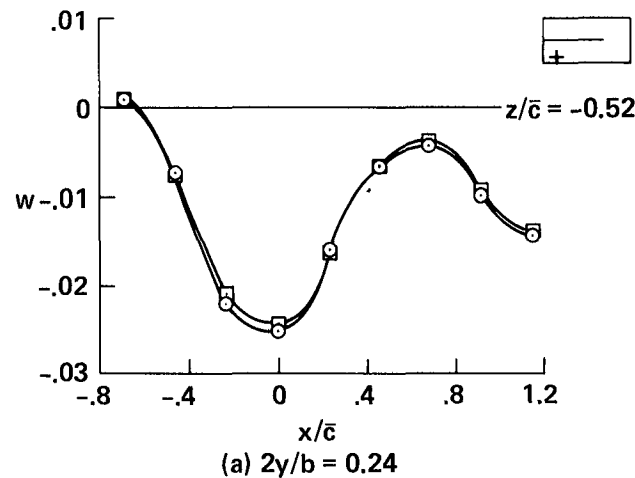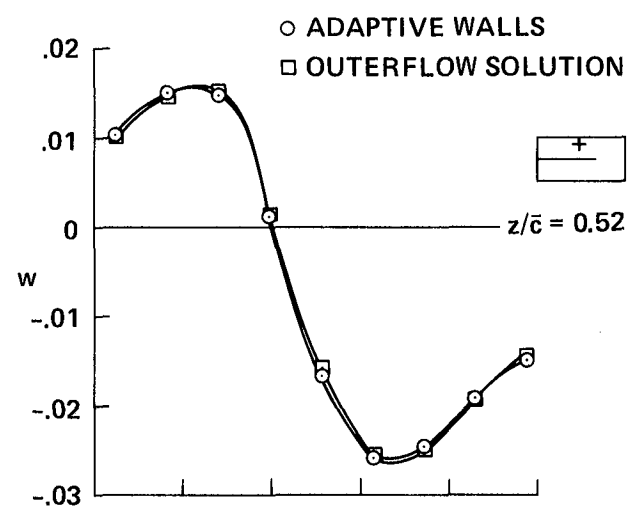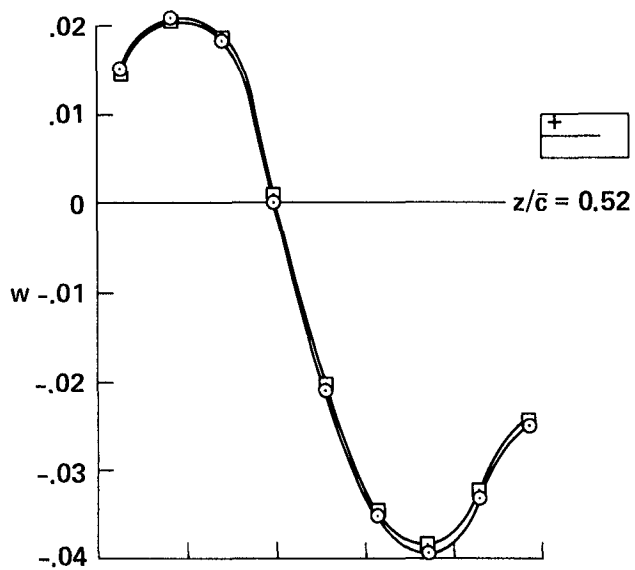
Figure 14.— Vertical velocities for the adaptive-wall wind tunnel, seventh iteration (series 2), C_L = 0.163.
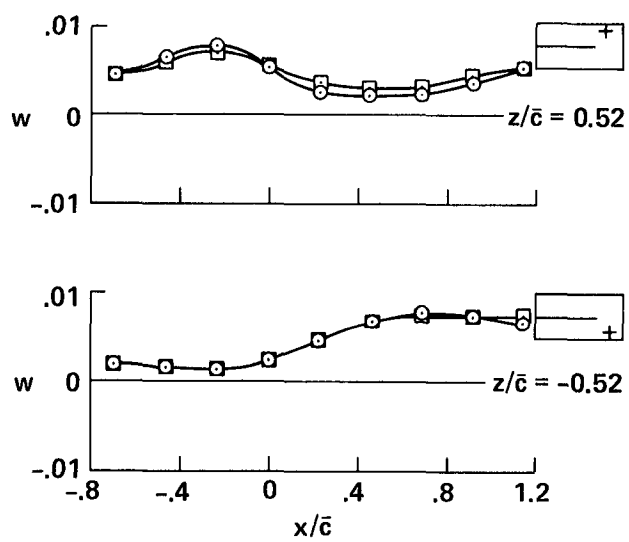
Figure 14.– Concluded.
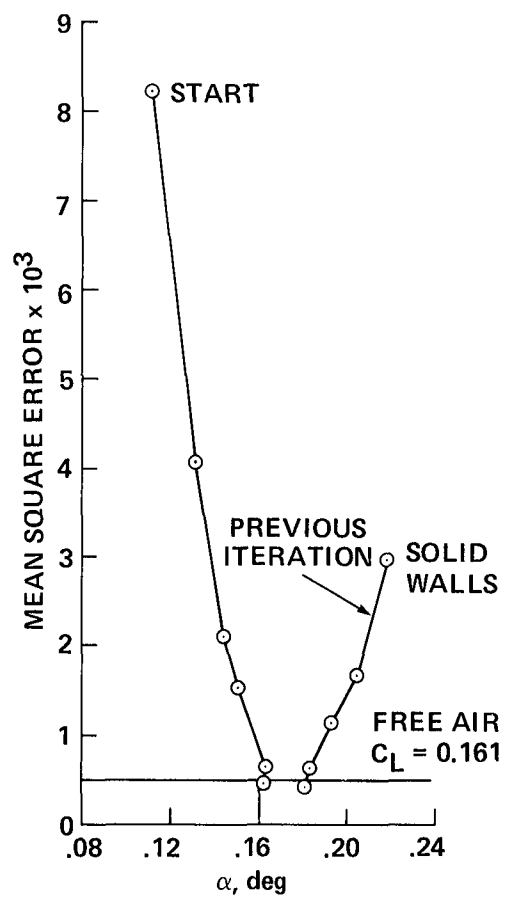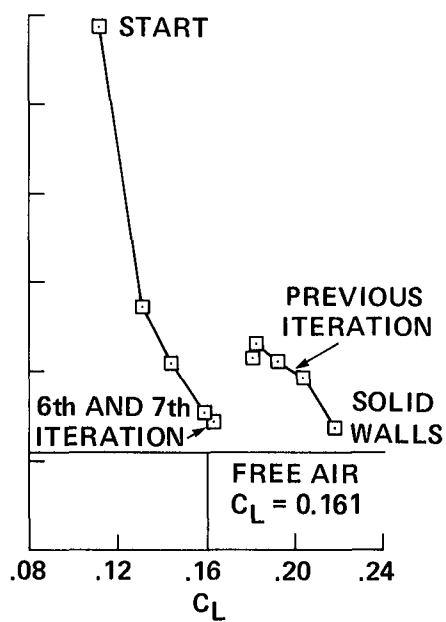
Figure 15.— Convergence rate.
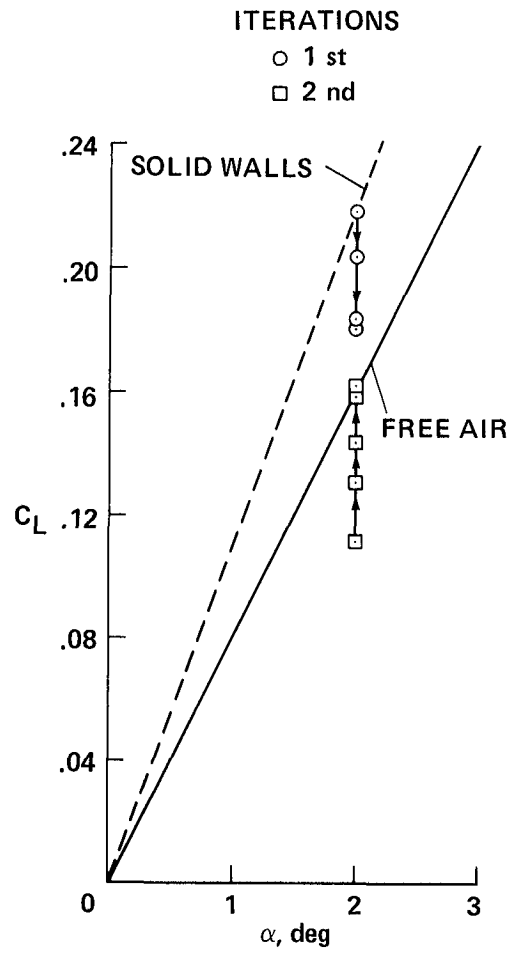
Figure 16.– Effect of iterations on C_L, $\alpha = 2°$.
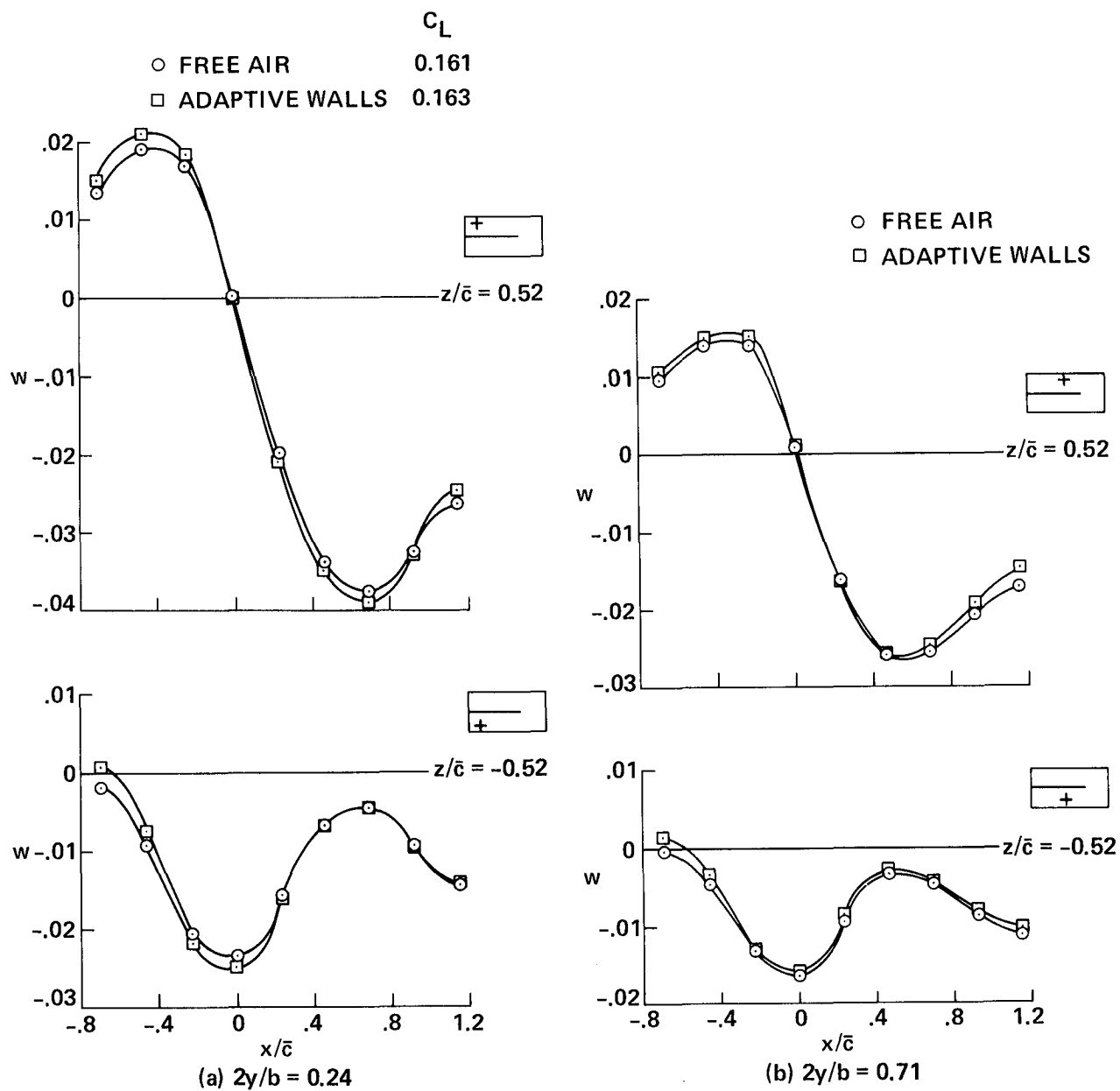
Figure 17.— Comparisons of free-air and adaptive-wall vertical velocities, $\alpha = 2°$.

(c) 2y/b = 1.18

(d) 2y/b = 1.30
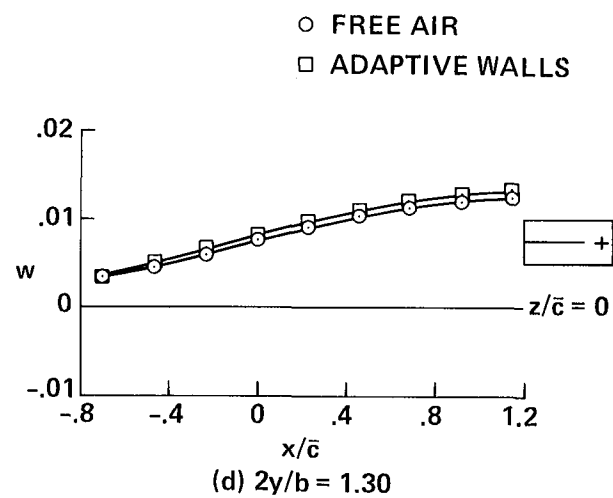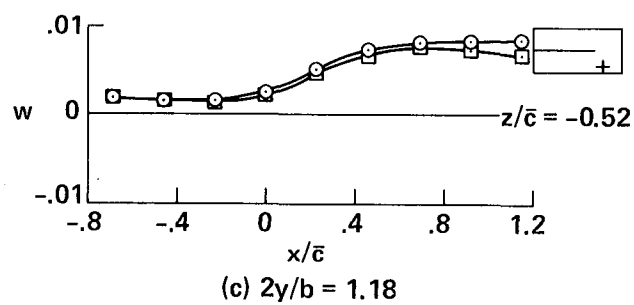
Figure 17.— Concluded.
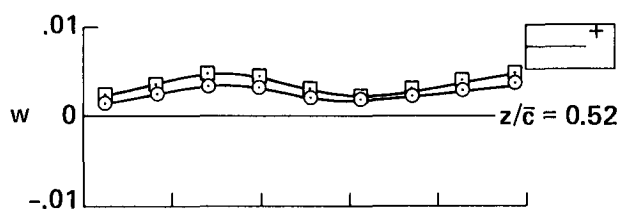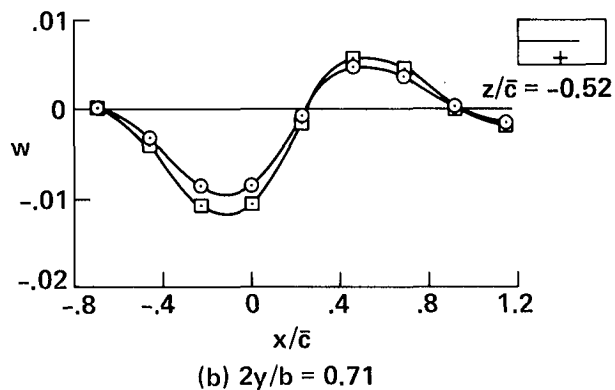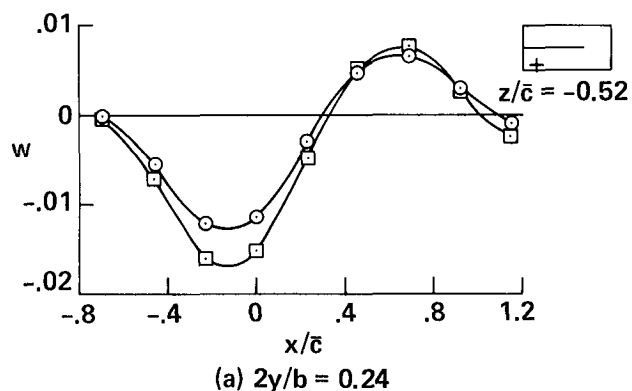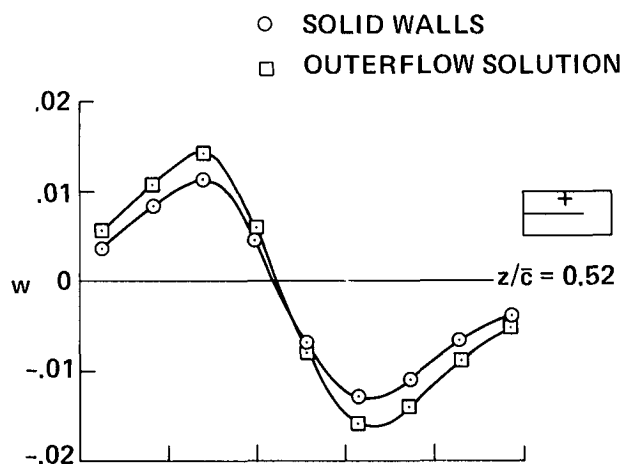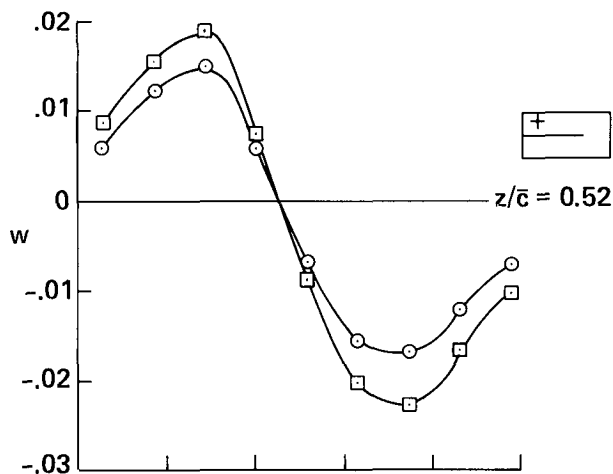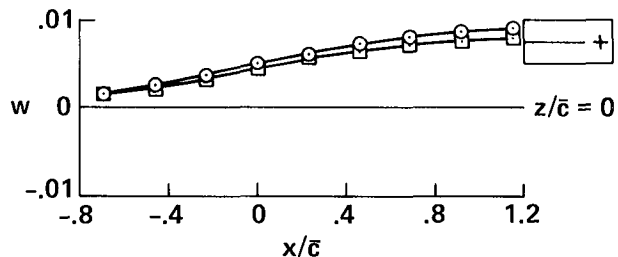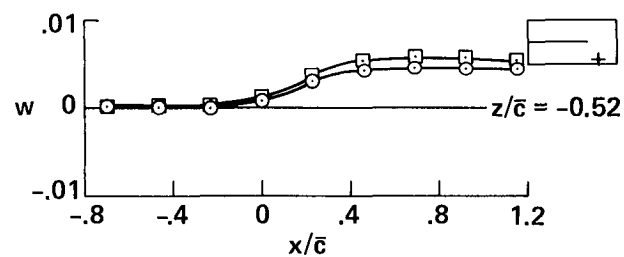
Figure 18.— Vertical velocities for the solid wall wind tunnel, $\alpha = 1°$, $C_L = 0.110$.
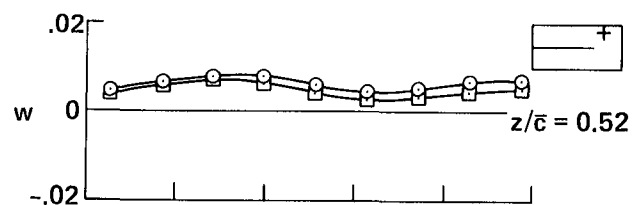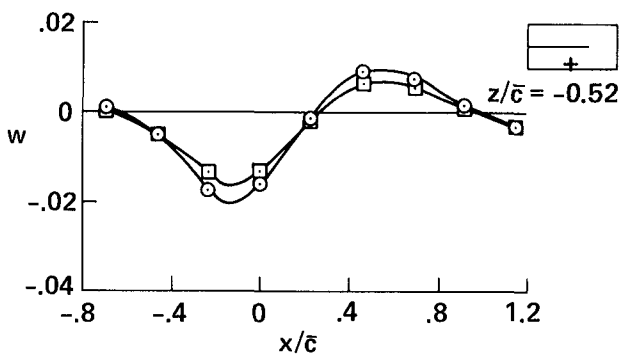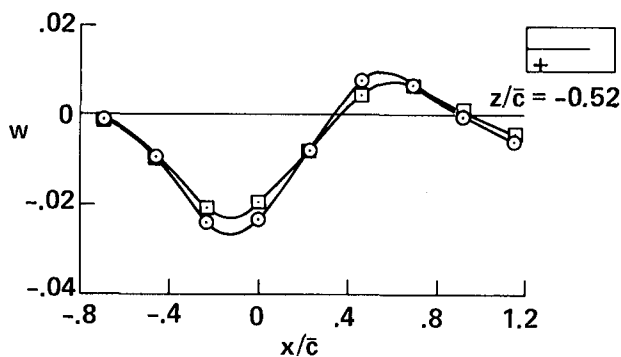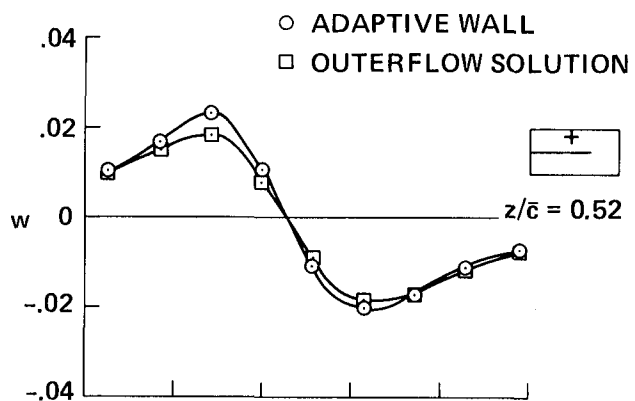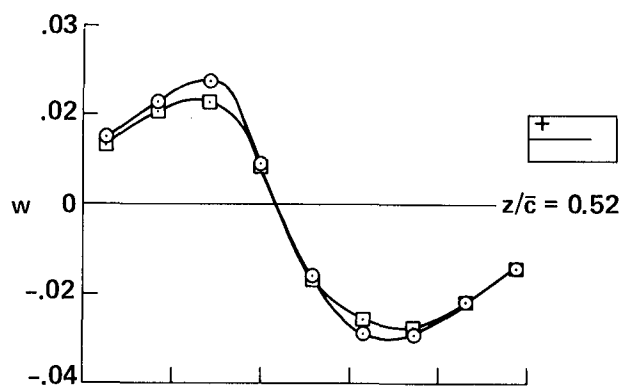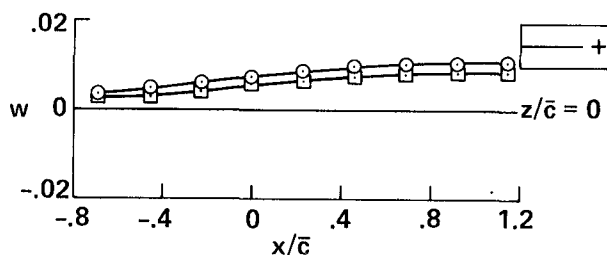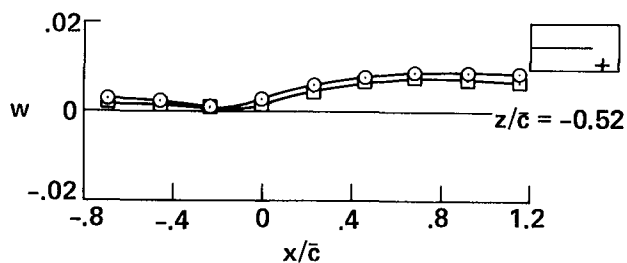
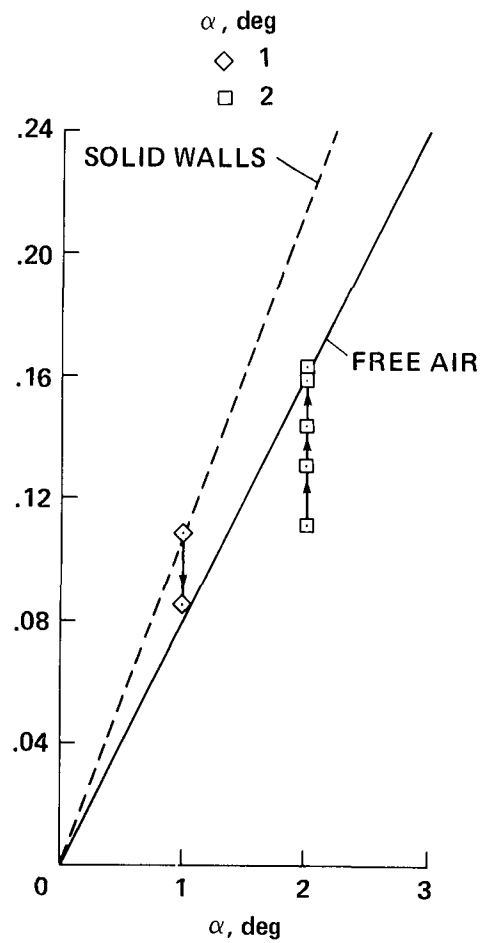Figure 19.— Vertical velocities for the adaptive-wall wind tunnel, $C_L = 0.086$.
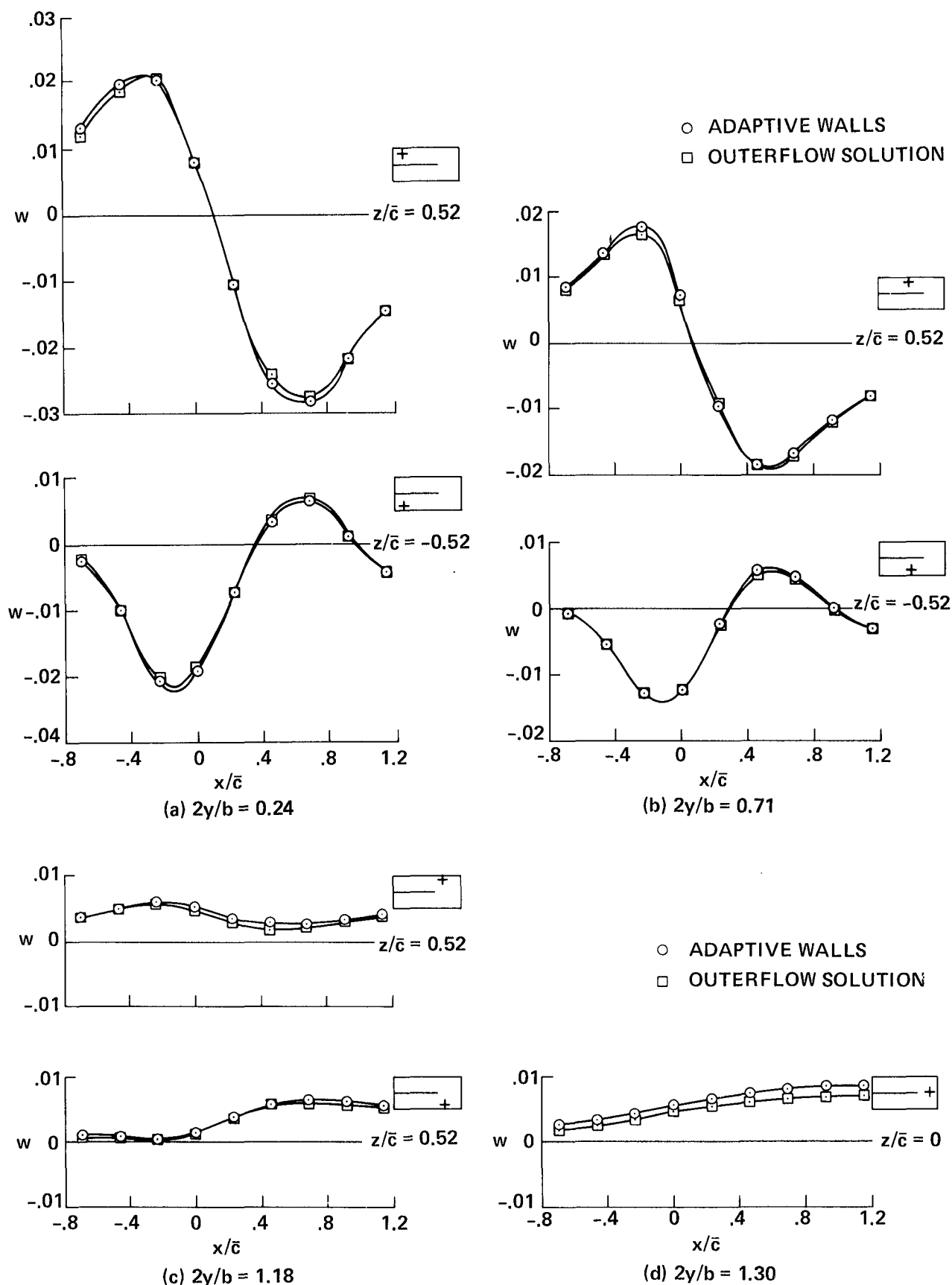
Figure 20.— Vertical velocities for the adaptive-wall wind tunnel, $C_L = 0.086$.
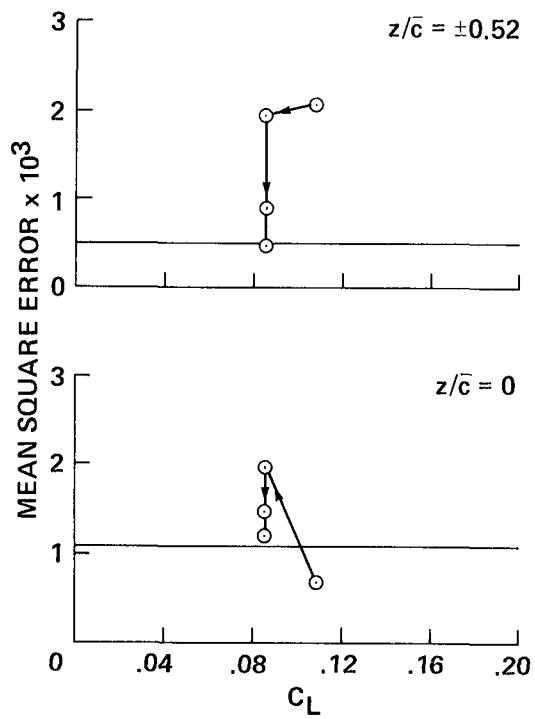
Figure 21.– Convergence rate.

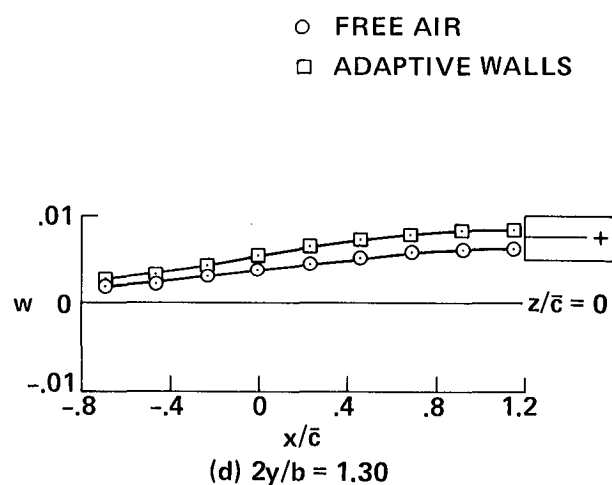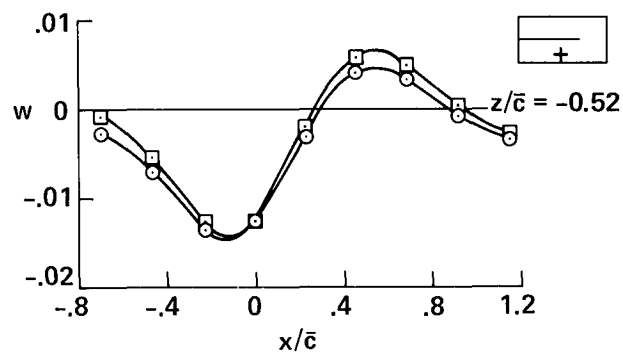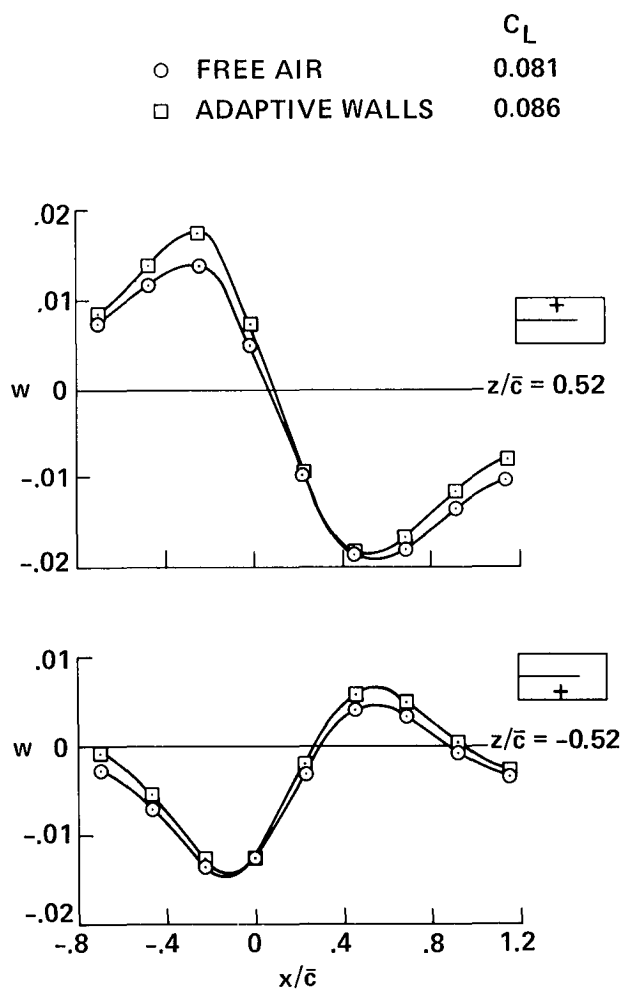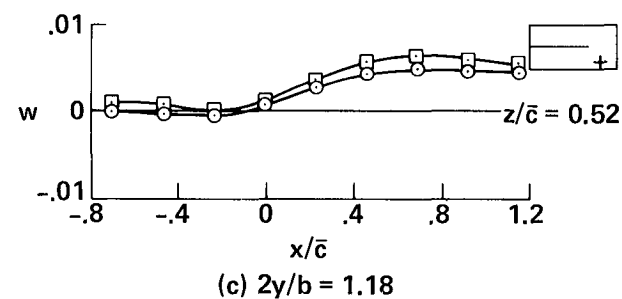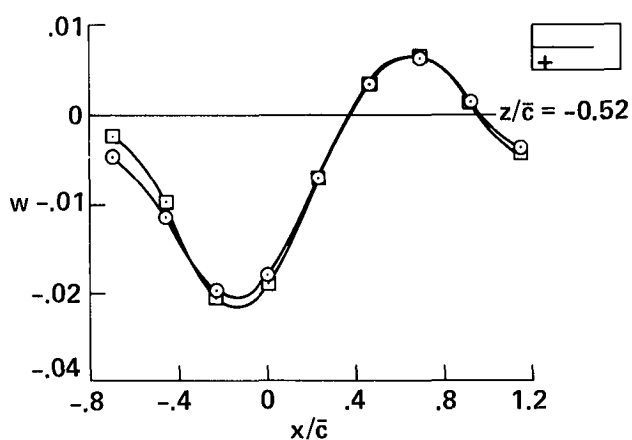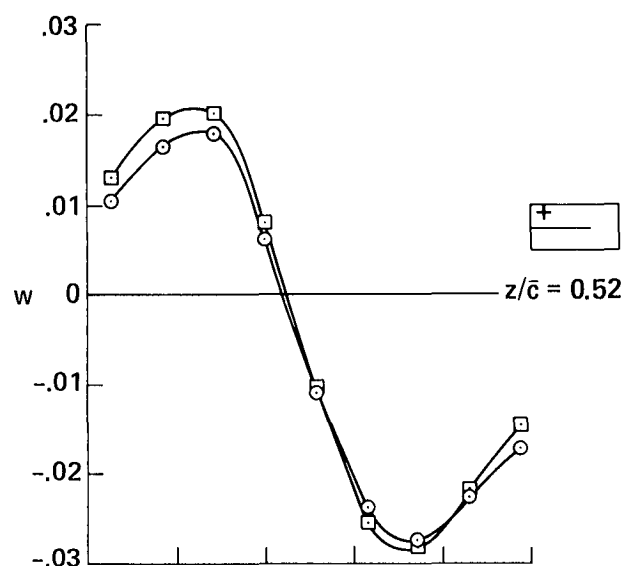

Figure 22.– Effect of iterations on C_L, $\alpha = 1°$.

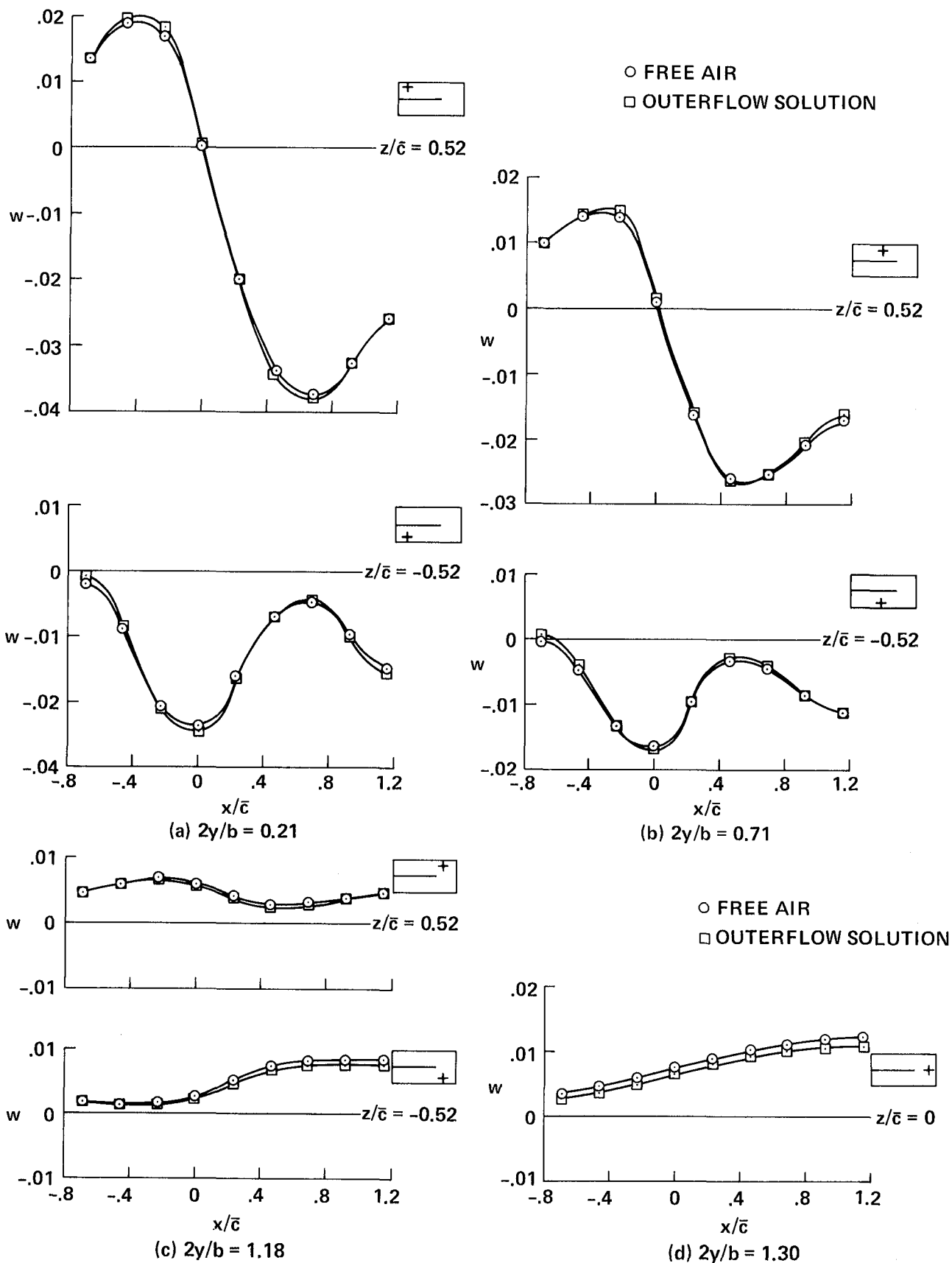Figure 23.— Comparisons of the free air and adaptive-wall vertical velocities, $\alpha = 1°$.

Figure 24.— Vertical velocities for interference-free flow, $C_L = 0.161$.

1. Report No. NASA TP-2351	2. Government Accession No.	3. Recipient's Catalog No.
4. Title and Subtitle A NUMERICAL SIMULATION OF THREE-DIMENSIONAL FLOW IN AN ADAPTIVE WALL WIND TUNNEL		5. Report Date August 1984
		6. Performing Organization Code
7. Author(s) J. P. Mendoza		8. Performing Organization Report No. A-9622
9. Performing Organization Name and Address Ames Research Center Moffett Field, CA 94035		10. Work Unit No. T-4613Y
		11. Contract or Grant No.
12. Sponsoring Agency Name and Address National Aeronautics and Space Administration Washington, DC 20546		13. Type of Report and Period Covered Technical Paper
		14. Sponsoring Agency Code 505-31-51

15. Supplementary Notes

Point of Contact: J. P. Mendoza, Ames Research Center, MS 227-8, Moffett Field, CA 94035
(415) 965-6288 or FTS 448-6288

16. Abstract

Numerical simulations of three-dimensional flows in a prototype adaptive wall wind tunnel were conducted at the Mach number of 0.6 to investigate: (1) wind-tunnel wall interference, (2) active streamline control by varying air removal or injection along the walls, and (3) to develop a method for establishing wall boundary conditions for interference-free flows. It was found that wind-tunnel wall interference could be controlled by using only the vertical velocity components. For the configuration tested, it was found that interference-free flow with solid sidewalls can be approximated by using only floor and ceiling blowing/suction.

17. Key Words (Suggested by Author(s)) Adaptive wall wind tunnel Outer flow solver Numerical flow simulation Wall interference	18. Distribution Statement Unclassified – Unlimited Subject Category – 02		
19. Security Classif. (of this report) Unclassified	20. Security Classif. (of this page) Unclassified	21. No. of Pages 35	22. Price* A02

National Aeronautics and
Space Administration

Washington, D.C.
20546

THIRD-CLASS BULK RATE

U.S.MAIL

NASA